

DFTB CALCULATIONS OF A SHAPELESS $Au_{55}(C_1)$ NANOCCLUSERS

K. Vishwanathan*

Physical and Theoretical Chemistry, University of Saarland, 66123 Saarbrücken, Germany

Abstract. We present a vibrational and heat capacity analysis of a shapeless (disordered) Au_{55} cluster. Our results show that several nonequivalent and nearly degenerate states, as well as, a triple and many double degeneracy states on the vibrational spectrum. The origin of the higher stability of the shapeless was in the short range of the n-body interaction existing in the clusters bonding. We have carried out the present ab initio study with DFTB by using the numerical finite-difference approach. Our calculations have confirmed with the experimental results, that is, a thermodynamically very stable structure can not be crystalline, but having a high probability of a shapeless structure. The non-crystalline structure of this cluster was validated by comparison (of the nuclei coordination numbers) with a different axis of rotations at a standard orientation of crystal shape. Significantly, we have accurately predicted the vibrational frequency range in between 3.41 to 335.78 cm^{-1} at $\Delta E = 0$. Nevertheless, our investigation have revealed that the vibrational spectrum and the heat capacity was very strongly influenced by the size, shape and the structure of the gold nanoclusters that are showing striking advances.

Keywords: Gold Atomic Clusters, Density-Functional Tight-Binding (DFTB) approach, finite-difference method, Force Constants (FCs), vibrational spectrum, heat capacity and boson peaks.

*Corresponding Author: K. Vishwanathan, Physical and Theoretical Chemistry, University of Saarland, 66123 Saarbrücken, Germany, Tel.: + 49-0151-63119680, e-mail: vishwa_nathan_7@yahoo.com

Received: 15 May 2019;

Accepted: 12 June 2019;

Published: 03 August 2019.

1. Introduction

Gold nanoparticles have attracted enormous scientific and technological interest due to their ease of synthesis, chemical stability, and unique optical properties. Proof-of-concept studies demonstrate their biomedical applications in chemical sensing, biological imaging, drug delivery, and cancer treatment. Knowledge about their potential toxicity and health impact is essential before these nanomaterials can be used in real clinical settings. Furthermore, the underlying interactions of these nanomaterials with physiological fluids is a key feature of understanding their biological impact, and these interactions can perhaps be exploited to mitigate unwanted toxic effects (Alkilany & Murphy, 2010). Surprisingly, Maria *et al.*, worked on gold clusters (Au_{55}) and shown to interact even with DNA. The experiments carried out armed with this knowledge have demonstrated that such clusters are shown to have significant toxicity towards many types of human cells, both healthy and cancerous, in contrast to previously studied larger gold nanoparticles. It is hoped, therefore, that there is a future for (Au_{55}) clusters in the treatment of certain cancers (Tsoli *et al.*, 2005).

Thus, among small size gold nanoparticles (NP), Au_{55} clusters possess an ideal size (1.4 nm) for catalytic activity, a full shell geometry, and oxidation-resistant properties (Simon *et al.*, 1993; Yam & Cheng, 2008; Murray, 2008; Jin, 2010; Periyasamy & Remacle, 2009). Several theoretical (Krakow *et al.*, 1994; Garzón & Jellinek, 1991; Sawada & Sugano, 1992; D'Agostino *et al.*, 1993; Yu & Duxbury,

1995) and experimental (Garzón & Jellinek, 1991; Marcus *et al.*, 1990; Pinto *et al.*, 1995) studies on the structure and stability of Au_n clusters have been reported in the literature (Garzón & Posada-Amarillas, 1996). Theoretical calculations based on the n-body Gupta potential suggest that the most stable structure of the Au_{55} cluster is icosahedral (Sawada & Sugano, 1992; D'Agostino *et al.*, 1993; Yu & Duxbury, 1995). On the other hand, the experimental information is still uncertain assigning cuboctahedral (Marcus *et al.*, 1990) and icosahedral (Pinto *et al.*, 1995) structures to such a cluster. Nevertheless, although the theoretical studies (Sawada & Sugano, 1992; D'Agostino *et al.*, 1993; Yu & Duxbury, 1995) agree about the higher stability of the icosahedral configuration with respect to the fcc cuboctahedron, none of them have explored the existence of other stable isomers with different symmetry, through a fully dynamical optimization procedure. However, the outcome is rather limited due to the fact that there are only sparse experimental results. The Au_{55} cluster is an exception, since this cluster, consisting of a magic number of atoms, is very stable. Consequently, some experimental data are available for comparison with predictions obtained by ab initio calculations. There are a few magic numbers indicating hypothetical closed-shell structures. The smallest one of these numbers is 13, with 12 atoms surrounding one central atom. The next two clusters with 55 or 147 atoms add one or two additional shells, respectively. In the outer shell, these clusters contain 42 atoms or 92 atoms, respectively. In the third magic cluster, the number of atoms in the outer shell is $147 - 55 = 92$ (Vollath & Fischer, 2014; Vollath *et al.*, 2017). Nevertheless, these clusters may be crystalline or non-crystalline.

Above all, since the most recent groundbreaking experimental work of Schmid's group (Schmid *et al.*, 1981; Schmid, 1985; Schmid, 2008; Benfield *et al.*, 1988; Cluskey *et al.*, 1993; Hornyak *et al.*, 1998), the Au_{55} cluster has been used as a model for the small cluster with a magic number of atoms. In their experimental work, and in particular the structural analysis, were possible only by attaching organic ligands to the cluster surface, in order to prevent the clusters from coagulating immediately to larger particles (Benfield *et al.*, 1988). Without any doubt, obtained by this way structural details do, to some extent, depend on the type of the ligands (Cluskey *et al.*, 1993); however, the structure is not influenced fundamentally. The important result of Schmid's work is the description of the structure of Au_{55} as a sequence of two shells (Schmid *et al.*, 1981; Cluskey *et al.*, 1993). On average, these clusters are composed of 13 atoms in the center and 42 atoms in the outer shell. From the atoms in the outer shell, 18 atoms are bonded to the ligands (Schmid *et al.*, 1981). Furthermore, these shells show a very broad scattering of the coordination numbers (Cluskey *et al.*, 1993). This fact was taken as an indication for a non-crystalline solid. Additionally, it was found that the bonding energy of these non-crystalline clusters is approximately 20 percent higher than that of bulk gold (Benfield *et al.*, 1988). These structural details were confirmed by Vogel *et al.* (1993). Both groups, Schmid *et al.* (Schmid *et al.*, 1981; Schmid, 1985; Benfield *et al.*, 1988; Cluskey *et al.*, 1993; Hornyak *et al.*, 1998; Schmid, 2008) and Vogel *et al.* (1993), described the shape of the Au_{55} cluster as cuboctahedral. It must be mentioned that there are also findings, especially related to the coordination numbers, that the Au_{55} cluster is possibly structurally close to the face-centered cubic (fcc) structure (Marcus *et al.*, 1990; Wallenberg *et al.*, 1985; Fairbanks *et al.*, 1990). Baletto & Ferrando (2005) prefer the term low symmetry structure instead of non-crystalline in their review article. Further experimental results going far beyond this short introduction, are summarized in a review by Schmid (2008).

Having this broad experimental background in mind, it is not surprising that a series of authors tried to describe the structure and the properties of Au_{55} clusters theoretically by means of molecular dynamics or ab initio modeling. These studies resulted in puzzling and often contradictory conclusions regarding the nanoparticle structure: crystalline vs non-crystalline, icosahedral vs cuboctahedral or even unspecific shapes. Doye & Wales (1998) described their resulting Au_{55} cluster with the lowest energy as non-crystalline and the structure of the neighboring Au_{56} cluster as fcc-based structure. Cox *et al.* (1999) interpreted their results as highly symmetric. In contrast, Michaelian *et al.* (1999) obtained a low-symmetry structure. Erkoç (2000) analyzed a series of gold clusters in the range from Au_{13} to Au_{55} concluding that the stability of these clusters increases with increasing similarity to the fcc structure. Similar results were obtained by Yildirim *et al.* (2006); these authors found that there is a series of isomers with small differences in the energy. For the central atom of an icosahedron they found a coordination number close to the ideal value of 12. A puzzling result was obtained by Darby *et al.* (2002) as they concluded the Au_{55} cluster had a non-crystalline structure, whereas the neighboring clusters Au_{54} and Au_{56} showed an fcc-based structure. A comparable result for the Au_{55} cluster was discussed by Li and co-workers (2000).

Additionally, Huang *et al.* (2008) and Wang L.M. & Wang L.S. (2012) strongly confirmed as an amorphous in their theoretical and experimental work as well as in the review article (Huang *et al.*, 2008; L.M. Wang & L.S. Wang, 2012). At the same time, very recently, Jian *et al.* (2015) confirmed that the Au_{55} cluster is an amorphous in their experimental research work. Their systematic structure analysis showed that a hybrid structure, predicted by density functional theory, best matches nearly half the clusters observed. Most other clusters are amorphous. Moreover, they believed that their conclusions are consistent with all the previous, apparently contradictory structural studies of the Schmid clusters (Schmid, 2008).

Considering this lack of a clear definition, one has to interpret the different results cum grano salis. Moreover, the long list of somewhat contradicting, and to some extent dis-satisfying, results on the structure of the Au_{55} nanocluster highlights the necessity to look again at this problem using up-to-date theoretical methods. Subsequently, to confirm the Au_{55} cluster is an amorphous or not, in this study, we use our numerical finite-difference approach along with density functional Tight-Binding (DFTB) method. Since our newly developed model has given a new deep insight of the clusters through the vibrational spectrum that has been already applied on the gold clusters with up to 20 (Vishwanathan, 2016; Vishwanathan, 2017a; Vishwanathan, 2017b; Vishwanathan, 2017c). At $\Delta E = 0$, the vibrational frequency of the optimized neutral gold cluster Au_{55} (Dong, 2006; Dong & Springborg, 2007) were extracted through re-optimization. The desired set of system eigenfrequencies ($3N - 6$) is obtained by a diagonalization of the symmetric positive semidefinite Hessian matrix. As well as, heat capacity and the boson peaks were plotted for the temperature influenced size effect. This computational process allows one to obtain detailed results with respect to the thermodynamic properties with quantum-mechanical accuracy.

2. Theoretical and Computational Procedure

The DFTB (Porezag *et al.*, 1995; Seifert & Schmidt, 1992; Seifert *et al.*, 1996) is based on the density functional theory of Hohenberg and Kohn in the formulation of

Kohn and Sham. In addition, the Kohn-Sham orbitals $\psi_i(\mathbf{r})$ of the system of interest are expanded in terms of atom-centered basis functions $\{\phi_m(\mathbf{r})\}$,

$$\psi_i(\mathbf{r}) = \sum_m c_{im} \phi_m(\mathbf{r}), \quad m = j. \quad (1)$$

While so far the variational parameters have been the real-space grid representations of the pseudo wave functions, it will now be the set of coefficients c_{im} . Index m describes the atom, where ϕ_m is centered and it is angular as well as radially dependant. The ϕ_m is determined by self-consistent DFT calculations on isolated atoms using large Slater-type basis sets.

In calculating the orbital energies, we need the Hamilton matrix elements and the overlap matrix elements. The above formula gives the secular equations

$$\sum_m c_{im} (H_{mn} - \epsilon_i S_{mn}) = 0. \quad (2)$$

Here, c_{im} 's are expansion coefficients, ϵ_i is for the single-particle energies (or where ϵ_i are the Kohn-Sham eigenvalues of the neutral), and the matrix elements of Hamiltonian H_{mn} and the overlap matrix elements S_{mn} are defined as

$$H_{mn} = \langle \phi_m | \hat{H} | \phi_n \rangle, \quad S_{mn} = \langle \phi_m | \phi_n \rangle. \quad (3)$$

They depend on the atomic positions and on a well-guessed density $\rho(\mathbf{r})$. By solving the Kohn-Sham equations in an effective one particle potential, the Hamiltonian \hat{H} is defined as

$$\hat{H}\psi_i(\mathbf{r}) = \epsilon_i \psi_i(\mathbf{r}), \quad \hat{H} = \hat{T} + V_{eff}(\mathbf{r}). \quad (4)$$

To calculate the Hamiltonian matrix, the effective potential V_{eff} has to be approximated. Here, \hat{T} being the kinetic-energy operator $\sum(\hat{T} = -\frac{1}{2}\nabla^2)$ and $V_{eff}(\mathbf{r})$ being the effective Kohn-Sham potential, which are approximated as a simple superposition of the potentials of the neutral atoms

$$V_{eff}(\mathbf{r}) = \sum_j V_j^0(|\mathbf{r} - \mathbf{R}_j|). \quad (5)$$

V_j^0 is the Kohn-Sham potential of a neutral atom, $\mathbf{r}_j = \mathbf{r} - \mathbf{R}_j$ is an atomic position, and \mathbf{R}_j being the coordinates of the j -th atom.

The short-range interactions can be approximated by simple pair potentials, and the total energy of the compound of interest relative to that of the isolated atoms is then written as,

$$E_{tot} \approx \sum_i \epsilon_i - \sum_j \sum_{m_j} \epsilon_{im_j} + \frac{1}{2} \sum_{j \neq j'} U_{jj'}(|\mathbf{R}_j - \mathbf{R}_{j'}|), \quad \epsilon_B \equiv \sum_i \epsilon_i - \sum_j \sum_{m_j} \epsilon_{im_j}. \quad (6)$$

Here, the majority of the binding energy (ϵ_B) is contained in the difference between the single-particle energies ϵ_i of the system of interest and the single-particle energies ϵ_{im_j} of the isolated atoms (atom index j , orbital index m_j), $U_{jj'}(|\mathbf{R}_j - \mathbf{R}_{j'}|)$ is determined as the difference between ϵ_B and ϵ_B^{SCF} for diatomic molecules (with ϵ_B^{SCF} being the total energy from parameter-free density-functional calculations). In the present study, only the $5d$ and $6s$ electrons of the gold atoms are explicitly included, whereas the rest are treated within a frozen-core approximation (Porezag *et al.*, 1995; Seifert *et al.*, 1996; Seifert, 2007; Warnke, 2007).

2.1. Structural re-optimization process

In our case, we have calculated the numerical first-order derivatives of the forces ($\mathbf{F}_{i\alpha}$, $\mathbf{F}_{j\beta}$) instead of the numerical-second-order derivatives of the total energy (E_{tot}). In principle, there is no difference, but numerically the approach of using the forces is more accurate,

$$\frac{1}{M} \frac{\partial^2 E_{tot}}{\partial \mathbf{R}_{i\alpha} \partial \mathbf{R}_{j\beta}} = \frac{1}{M} \frac{1}{2ds} \left[\frac{\partial}{\partial \mathbf{R}_{i\alpha}} (-\mathbf{F}_{j\beta}) + \frac{\partial}{\partial \mathbf{R}_{i\beta}} (-\mathbf{F}_{j\alpha}) \right]. \quad (7)$$

Here, $k = (\mathbf{F}_{j\alpha}, \mathbf{F}_{j\beta})$ is a restoring force which is acting upon the atoms, ds is a differentiation step-size and M represents the atomic mass, for homonuclear case. The complete list of these force constants (FCs) is called the Hessian H , which is a $(3N \times 3N)$ matrix. Here, i is the component of (x, y or z) of the force on the j 'th atom, so we get $3N$.

Differentiation step-size (ds) on the Potential Energy Surface: We found that the differentiation on the single point energy (SPE) of the equilibrium coordinates of the optimized cluster for a small step-size [$ds = \pm 0.01$ a.u.], which has been approached through the scheme developed by M. Dvornikov (2003) with DFTB calculations. Moreover, we have confirmed that it would be a very reasonable value that has allowed to discriminate between the translational, rotational motion (Zero-eigenvalues) and the vibrational motion (Non-Zero-eigenvalues) of the atoms (or molecules) of the Hessian eigenvalues (Vishwanathan, 2018).

2.2. Calculation of the heat capacity of the clusters

The specific heat capacity is a measurable physical quantity that characterizes the ability of a body to store the heat when the sample temperature is changed. The effect of body size on the specific heat capacity has recently attracted a lot of attention (Warnke, 2007; Novotny *et al.*, 1972; Song *et al.*, 2004; Yao *et al.*, 2005; Jun *et al.*, 2005). Now we proceed to calculate the specific heat contribution due to the vibrational energy.

The Helmholtz free energy

$$F = U - TS \quad (8)$$

of the system can be expressed in terms of its partition function Z .

U is the internal energy of the system or clusters, T is the absolute temperature and S is the entropy (or) the better way of re-writing for our calculation

$$U_{vib} = F_{vib} + TS_{vib}, \quad (9)$$

where U_{vib} denoting the vibrational energy of the system of the $(3N - 5)$ or $(3N - 6)$ independent harmonic oscillators.

For the moment, we only need to focus on the vibrational part of the free energy. We start from $F_{vib} = -kT \ln(z)$ and let in eqn. below,

$$Z_{vib} = \prod_{i=1}^{NVM} \left[2 \sinh \left(\frac{\alpha_i}{2} \right) \right]^{-1} \quad (10)$$

NVM is the number of normal vibrational modes of the cluster. The above calculations were used to examine the Helmholtz free energy of the clusters as a function of temperature.

$$F_{vib} = -kT \ln \left(\prod_{i=1}^{NVM} \left[2 \sinh \left(\frac{\alpha_i}{2} \right) \right]^{-1} \right), \quad \alpha_i = \frac{\hbar \omega_i}{k_B T}. \quad (11)$$

Here, \hbar is the reduced Planck's constant and k_B is Boltzmann's constant, so the vibrational contribution to the free energy is

$$F_{vib} = kT \sum_{i=1}^{NVM} \left[\frac{\alpha_i}{2} + \ln(1 - e^{-\alpha_i}) \right]. \quad (12)$$

Furthermore, we see that

$$\ln(z) = - \sum_{i=1}^{NVM} \left[\frac{\alpha_i}{2} + \ln(1 - e^{-\alpha_i}) \right] \quad (13)$$

We make use of the relation, to write

$$S_{vib} = - \left(\frac{\partial F}{\partial T} \right)_V \quad (14)$$

$$S_{vib} = \left(\frac{\partial}{\partial T} [kT \ln(z)] \right)_V = k \ln(z) + kT \left(\frac{\partial \ln(z)}{\partial T} \right)_V$$

As we mentioned before, since heat capacity of a material is directly related to the atomic structure, measurements of heat capacity as a function of temperature could indicate the structural message of nanostructured materials. The vibrational frequencies depend on the molecules structure.

The vibrational contribution to the heat capacity of the system of interest is the derivative of the vibrational energy with respect to the temperature. It can be calculated as,

$$C_{vib} = \frac{\partial U_{vib}}{\partial T}. \quad (15)$$

From above equations (9-14) the vibrational energy of the system of $(3N - 5)$ or $(3N - 6)$ independent harmonic oscillators can be written as

$$U_{vib} = kT \sum_{i=1}^{NVM} \left[\frac{\alpha_i}{2} + \frac{\alpha_i}{e^{\alpha_i} - 1} \right]. \quad (16)$$

Combining the last two equations (15) and (16) eventually yields an equation linking together the set of eigen-frequencies of the cluster and its vibrational heat capacity:

$$\frac{\partial U_{vib}}{\partial T} = \frac{\partial}{\partial T} \left[kT \sum_{i=1}^{NVM} \left(\frac{\alpha_i}{2} + \frac{\alpha_i}{e^{\alpha_i} - 1} \right) \right]. \quad (17)$$

Finally, we can get the formula to investigate size, structure and temperature effects on the heat capacity of clusters,

$$C_{vib} = \frac{1}{N} \sum_{i=1}^{NVM} \frac{\alpha_i^2 e^{\alpha_i}}{(e^{\alpha_i} - 1)^2}; \quad \alpha_i = \frac{\hbar \omega_i}{k_B T}, \quad (18)$$

$$\alpha_i = \omega_i / (0.6950356 * T),$$

$$\alpha_i = \omega_i / T,$$

and C_{vib}/T^3 vs T (for the Boson Peaks),

$$0.6950356 = [h(6.626 \times 10^{-34} J - s) c(2.9979 \times 10^{10} cm - s^{-1}) / k_B(1.380 \times 10^{-23} J - K^{-1})]^{-1}.$$

Zero vibrational modes are excluded from the summation in eqn. (18), where N is the size of the atomic clusters.

3. Results and Discussion

In order to fully exploit the potential applications of cluster based nanomaterials, it is necessary to gain full control of the cluster size, shape and the structure. Therefore, in this article, we present an in-depth study on the behavior of vibrational frequency (at $\Delta E = 0$), as well as, heat capacity of the re-optimized neutral gold cluster (Au_N , $N = 55$). We found that the vibrational frequency and the heat capacity of the cluster was very strongly depending upon the structure, shape and mainly influenced by the size.

3.1. The optimized structure of the cluster Au_{55}

At first, the structures were optimized through a so called genetic algorithm (GA) in combination with parameterized Density Functional Tight-Binding (DFTB) energy calculations and a steepest descent algorithm permitting a local total energy minimization. It is given some general information about global minima gold structures, which have been revealed by the work of Yi Dong (2006) and Dong & Springborg (2007). Nevertheless, Au_{55} symmetric structure is C_1 , but it is always depends upon the ground state minimum-energy isomer (see Fig. 1). The results were compared with jellium calculations and with those of earlier embedded-atom studies, it was demonstrated that for gold atomic clusters, electronics effects are very important, leading to a partly suppression of the occurrence of magic numbers, as well as to low-symmetry and only partly compact clusters. In addition to that the shell-like structure was found. Moreover, Häkkinen *et al.* (2004) and other researchers (Ignacio *et al.*, 1996; Huang *et al.*, 2008; Wang L.M. & Wang L.S., 2012; Jian *et al.*, 2015) found that for $53 \leq N \leq 58$, low-symmetry, ‘amorphous structure’ were found, which they ascribed to strong relativistic effects. Although, Dong & Springborg (2007) calculations, the relativistic effects are only partly included, but very similar results are nevertheless found. Surprisingly, they found that it has a relatively low symmetry (and not an icosahedral, cuboctahedral or dodehahedral symmetry, as other researchers assumed and found) with one atom at the center of a slightly distorted high-symmetric structure. Their different analysis suggested that there is no fragments of the crystal are found.

Here, for the better understanding, we discuss some additional information of the optimized clusters which has not been dealt before. Since the optimization procedure does not guarantee that the lowest-energy Au_{55} amorphous cluster corresponds to the global minimum of the PES, it could be possible that ordered or highly symmetric structures other than the icosahedron or cuboctahedron exist with lower energy values. In our case, the total energy as a function of size of the cluster, is approximately, $E_B(N) = 4.95 \text{ eV/atom}$ for Au_{55} , with a very stable structure having with only one isomer (Dong, 2006). Moreover, the total energy differences of various clusters are relatively small. However, a noncrystalline cluster will certainly have some short-range order but that lacks the long-range order that is characteristic of a crystal.

Very particularly, since there is no spin-polarizations included with DFTB calculations, therefore, the gap E_g between the highest occupied and the lowest un-

occupied orbital (HOMO and LUMO) vanishes for odd N , that means there is no fluctuations at all. Nevertheless, for odd N , considerably two other gaps, one between the single-occupied orbital and the lowest completely empty orbital, $E_{g,1}$, and the other one between the highest completely filled orbital and the single-occupied one, $E_{g,2}$. Therefore, there is no chance to have, either icosahedral or cuboctahedral shapes (Dong, 2006; Dong & Springborg, 2007).

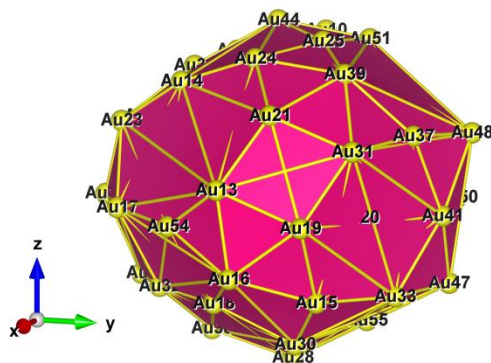


Figure 1. Style (Polyhedral), Optimized structure of the cluster $Au_{55}(C_1)$: Standard orientation of the crystal shape

The term genetic algorithm is used for a class of computational tools searching for the global minimum on the PES (Joswig, 2003). The PES is nothing else but a mapping, assigning a total energy value to a given nuclear configuration $s \in \mathfrak{R}^{(3N-6)}$. Since their underlying philosophy is based on the Darwinian evolution theory, they are given the name genetic or evolutionary algorithms. They were first introduced by Holland, who tried to improve the understanding of natural adaptation processes by designing artificial systems exhibiting properties similar to the ones of their natural equivalents (Holland, 1975; Goldberg, 1989). The strategy of the genetic algorithms is to try to avoid the generation and calculation of structures which are energetically irrelevant and to converge as fast as possible towards the lowest possible energy without missing the global minimum, by a mathematical formulation of the idea of the survival of the fittest. There is a multitude of different realizations of genetic algorithms (Deaven & Ho, 1995; Morris *et al.*, 1996; Roberts *et al.*, 2000; Hartke, 1995). Some of them are reviewed in the thesis of Jan-Ole Joswig (2003). At the end, we have confirmed the shapeless structure of $Au_{55}(C_1)$, through the size effect which influenced on the vibrational heat capacity.

Notice that the disordered isomers are more stable than the high symmetry icosahedron and cuboctahedron clusters. The higher stability of disordered metal cluster isomers with respect to symmetric ordered structures was also found in Al_{55} using the ab initio Car-Parrinello method (Yi *et al.*, 1991) and in Pt_{55} with an EAM potential (Sachdev *et al.*, 1993). This behavior contrasts with the one observed in the $(KCl)_{32}$ ionic cluster where the rock-salt crystalline structure is more stable than the amorphous isomers (Rose & Berry, 1993). Rare-gas atom clusters modeled with a Lennard-Jones potential also have a highly symmetric icosahedral structure as the lowest-energy configuration for $n = 55$ and other magic numbers (Garzón & Jellinek, 1991; Jellinek & Garzón, 1991).

On the other hand, Wang & Palmer (2012) have been reported the atomic-scale structures and fluctuating dynamical behavior of size-selected Au_{55} clusters obtained by

aberration-corrected scanning transmission electron microscopy (STEM) coupled with systematic STEM simulations. No high-symmetry structures (face-centered cubic polyhedron, icosahedron, or decahedron) were observed in their statistical investigation. They found Au_{55} clusters that are characteristic of the theoretically predicted chiral structure and similar sister isomers (which together they define as the chiral structural zone). The chiral structural zone was found to arise repeatedly in the time-lapse sequences of images they measured, though other amorphous-like structures are also frequently observed.

In addition to these reports based primarily on X-ray diffraction and EXAFS measurements, studies using high-resolution electron microscopy (Marcus *et al.*, 1990; Wallenberg *et al.*, 1985; Fairbanks *et al.*, 1990) were performed. Importantly, these studies pointed out that the structure of small gold clusters was unstable; rather fluctuations between different shapes, primarily, between icosahedral and cuboctahedral habitus were observed (Wallenberg *et al.*, 1985). A theoretical description of these fluctuations was given by Sawada & Sugano (1990). Howsoever, these authors indicated that the appearance of the cuboctahedral structure has a low probability at room temperature. Based on the experimental studies it can be concluded that an icosahedrally shaped cluster was never observed and, astonishingly, even when these clusters are not crystalline, they have a higher bonding energy than bulk gold (Jian *et al.*, 2015).

Garzón & Posada-Amarillas (1996) presented a structural and vibrational analysis of several amorphous (disordered) and ordered isomers of a Au_{55} – atom gold cluster. A Gupta n-body potential, with parameters fitted to gold clusters was used to model the metallic bonding in the Au_{55} cluster. The molecular-dynamics method combined with simulated annealing and quenching techniques were used to perform the cluster structure optimization. Their results show that several nonequivalent and nearly degenerate in energy amorphous cluster structures are more stable than those with high symmetry like the Au_{55} – atom Mackay icosahedron and the fcc cuboctahedron. The calculated distribution of normal frequencies clearly discriminates between amorphous and ordered cluster configurations and confirms their stability. A common-neighbor analysis was implemented to characterize the disordered cluster structures, identifying the short-range order of the amorphous phase, according to the local environment of each atom pair in the cluster. Distorted multilayered icosahedral order was found to be the more representative of the amorphous clusters with the lowest energies. At higher energies, the amorphous structures are characterized by the presence of distorted local icosahedral order. The origin of the higher stability of shapeless vs ordered isomers in Au_{55} is in the short range of the n-body interaction existing in the metal cluster bonding.

There are other interesting features in the vibrational properties of the Au_{55} clusters. The vibrational spectra of the amorphous isomers are shifted to lower frequencies with respect to the icosahedron normal modes distribution. This makes the amorphous clusters less stiff than the icosahedral isomer. Aside from the clear difference between ordered and disordered cluster configurations given through their frequency spectra, some differences are also displayed between the vibrational modes distribution of amorphous clusters. In particular, it is notorious that in the lowest-energy isomer with a configuration not far from the icosahedron, there exists a high

density of modes toward the middle of the distribution, whereas in the more disordered third lowest lying isomer the frequency distribution is more homogeneous along the whole range of frequencies (Garzón & Posada-Amarillas, 1996).

In our case, the cluster atomic configurations can be used to evaluate the second derivatives of the potential energy with respect to the atomic coordinates. These values generate the elements of the dynamical matrix. A numerical diagonalization of this matrix was performed to obtain the normal mode frequencies and eigenvectors. Six of the calculated $3N$ eigenvalues are equal to zero, corresponding to translational and rotational motions. The remaining $(3N - 6)$ frequencies are the vibrational normal modes. Table 1 shows clearly the normal mode vibrational frequencies distribution of the amorphous Au_{55} isomers. The detailed depth information can be explained as below.

Table 1. Normal vibrational modes (NVM [$3N - 6$]) and the vibrational frequency (ω_i) [in cm^{-1}] of the cluster Au_{55} at $\Delta E = 0$.

NVM (3N-6)	ω_i [cm^{-1}]						
1	3.41	43	42.59	85	94.95	127	184.21
2	3.69	44	43.2	86	96.07	128	186.95
3	5.6	45	43.35	87	98.41	129	192.3
4	8.03	46	44.42	88	100.05	130	193.53
5	8.41	47	45.95	89	101.76	131	194.87
6	9.66	48	47.21	90	104.02	132	196.39
7	10.52	49	48.15	91	104.81	133	201.87
8	11.52	50	48.99	92	110.7	134	203.15
9	12.28	51	50.18	93	111.35	135	204.15
10	12.87	52	50.56	94	113.78	136	204.89
11	12.95	53	51.92	95	114.19	137	207.07
12	13.86	54	54.39	96	116.79	138	210.86
13	15.14	55	54.6	97	117.38	139	214.44
14	15.34	56	55.8	98	119.96	140	217.91
15	16.27	57	57.08	99	123.52	141	221.94
16	17.79	58	59.44	100	124.58	142	225.44
17	18.87	59	59.8	101	127.49	143	227.84
18	19.73	60	60.42	102	130.44	144	231.47
19	19.94	61	61.59	103	132.49	145	235.02
20	20.81	62	61.78	104	134.09	146	236.99
21	21.32	63	62.69	105	135.41	147	241.26
22	22.04	64	66.11	106	137.8	148	243.73
23	22.66	65	66.49	107	139.67	149	249.35
24	23.18	66	67.6	108	142.34	150	250.62
25	24.83	67	67.89	109	143.4	151	254.83
26	25.33	68	69.62	110	149.25	152	258.44
27	26.56	69	71.38	111	151.09	153	261.6
28	26.92	70	73.97	112	153.41	154	264.34
29	27.94	71	74.41	113	155.45	155	265.44

30	29.82	72	75.1	114	157.63	156	277.04
31	29.97	73	76.44	115	159.59	157	282.88
32	31.03	74	77.32	116	159.97	158	300.76
33	32.04	75	79.61	117	163.95	159	335.78
34	34.27	76	80.96	118	165.37	-	-
35	34.88	77	81.69	119	167.59	-	-
36	35.31	78	83.46	120	170.11	-	-
37	36.43	79	84.27	121	171.25	-	-
38	37.14	80	88.66	122	173.07	-	-
39	38.06	81	89.63	123	175.94	-	-
40	39.2	82	89.94	124	178.01	-	-
41	40.92	83	92.94	125	179.92	-	-
42	41.6	84	94.53	126	181.63	-	-

3.2. The vibrational frequency (ω_i) ranges of the cluster Au_{55} at $\Delta E = 0$

Table 1 shows that the low (at the least) and the high (at the most) frequency range of cluster Au_{55} . The lowest and the highest frequency range in between 3.41 cm^{-1} to 335.78 cm^{-1} .

Firstly, the cluster has some low frequencies ω_{min} in between $3.41 - 9.66 \text{ cm}^{-1}$, that is only for the first 6 NVM, which comes even below the scale of Far Infrared FIR, IR-C 200 – 10 cm^{-1} .

Secondly, the frequency ranges are in between $10.52 - 196.39 \text{ cm}^{-1}$ for the 7 – 132 NVM, which come within the range of Far Infrared FIR, IR-C 200 – 10 cm^{-1} .

Thirdly, for the rest of the NVM 133-159, the maximum high frequency (ω_{max}) – $201.87 - 335.78 \text{ cm}^{-1}$) falls within the range of Mid Infrared MIR, IR-C 3330 – 200 cm^{-1} .

3.3. The double and the triple state degeneracy of the cluster Au_{55} at $\Delta E = 0$

The vibrational spectra of eigenvalues were found in the region between 3.41 and 335.78 cm^{-1} . We have observed that the most of the eigenvalues (114) are non-degenerate (single state) vibrations with respect to the NVM. Moreover, an exciting phenomena of the excellent motions of the atoms (some) within the clusters, particularly, 45 out of 159 of the normal modes has released 21 pairs of double-fold and only one set of three-fold state degeneracy [NVM 9, 10, 11 \rightarrow (12.28, 12.87, 12.95) cm^{-1}] occurred (see Table 1), most interestingly even at the beginning of the normal mode vibrations. This gives a very strong confirmation of the energy can be observed and be released with the same amount that corresponds to a certain local bond length rearrangements. A very interesting and excited things to be noticed that the first 2 pairs of double-fold degeneracy occurs below the scale of Far Infrared FIR, IR-C 200 – 10 cm^{-1} . Such kind of frequencies may not be possible to observe in the experimental calculations or will be silent.

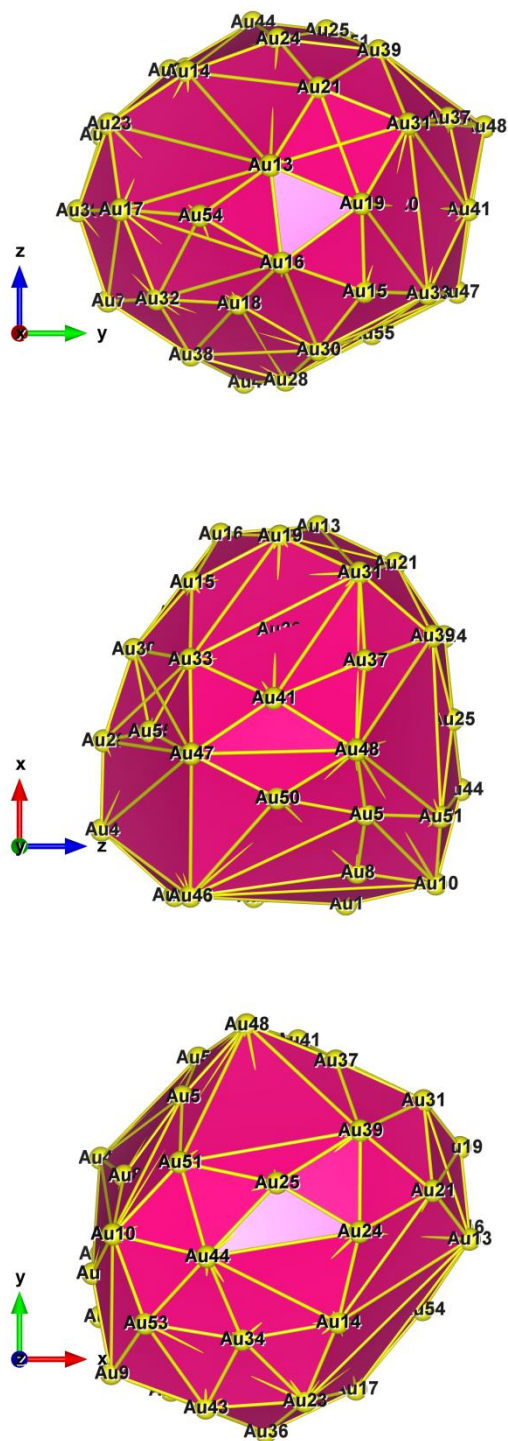


Figure 2. Style (Polyhedral), $Au_{55}(C_1)$: View along the a -axis, View along the b -axis and View along the c -axis (from top to bottom)

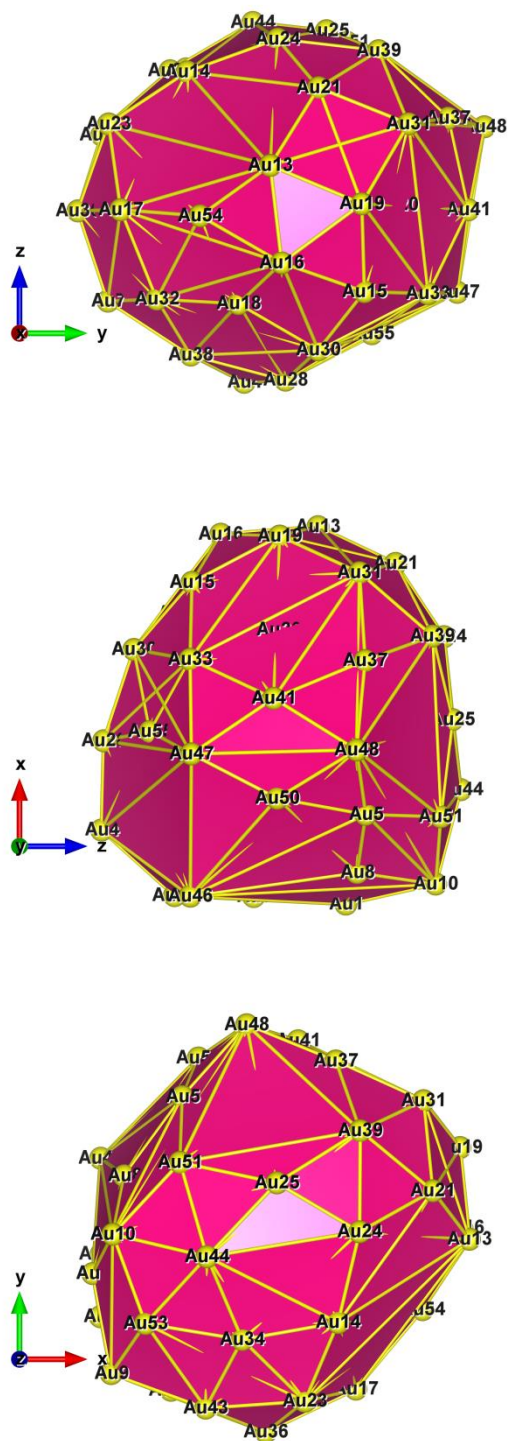


Figure 3. Style (Polyhedral), $Au_{55}(C_1)$: Rotate around the a^* -axis, Rotate around the b^* -axis and Rotate around the c^* -axis (from top to bottom)

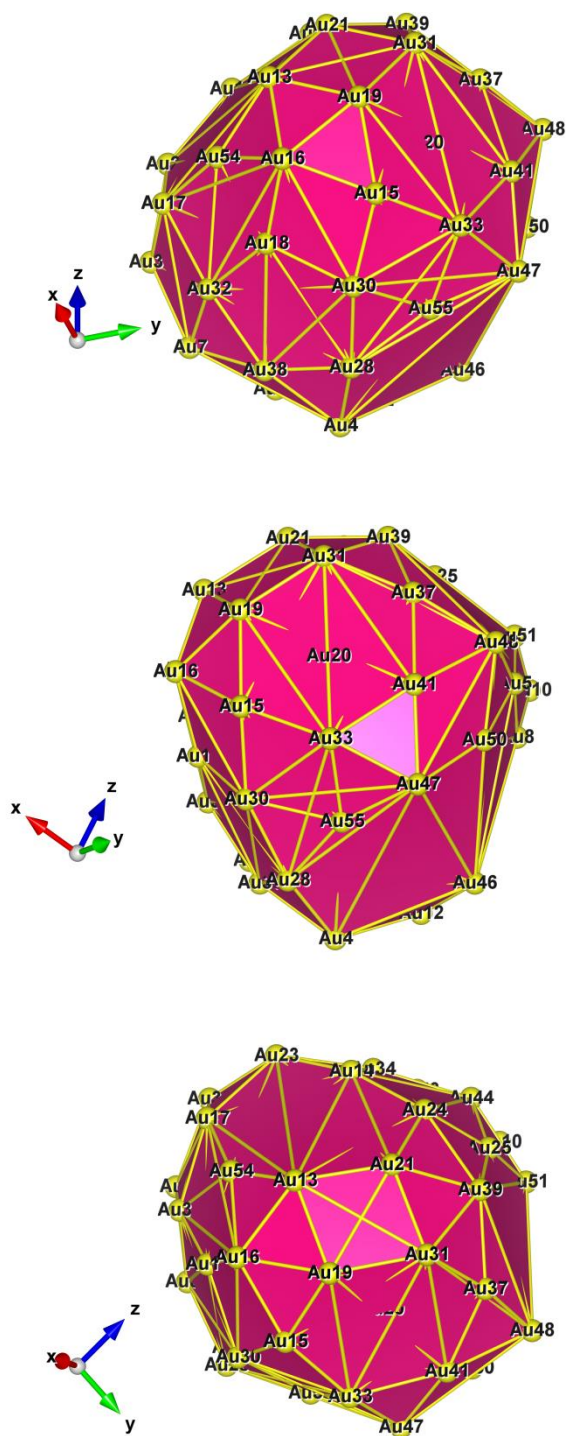


Figure 4. Style (Polyhedral), $Au_{55}(C_1)$: Rotate around the X-axis, Rotate around the Y-axis and Rotate around the Z-axis (from top to bottom)

Structural view of the shapeless $Au_{55}(C_1)$ structures: In one case, from the Figs. 2, 3; we are looking down the direct space a , b , or c axis and in the other case we are looking down the reciprocal space a^* , b^* and c^* axes. Since the axis of Cartesian coordinates does not have any changes, because it is not a crystal structure. By the way, we have also shown the structure is being rotated around the X -axis, the Y -axis and the Z -axis (see Fig. 4) [See the number of faces, vertices and edges]. Over all, in the perspective view the shell-like structures are found. It is suggested that the ability of gold to form strong binding in low-coordinated systems is the reason for the occurrence of shell-like structures. This cluster is composed of two shells surrounding a central atom.

Peculiarly, the optical absorption of bare and ligand-coated Au_{55} and Au_{69} Schmid clusters were calculated using time-dependent density functional theory. Calculations were performed using the explicit time propagation method with the local density approximation for the exchange-correlation potential. Both icosahedral and cuboctahedral structures of the Au_{55} gold core were simulated. The ligand coating was shown to have the effect of reducing the features of the optical absorption spectrum of the clusters, giving a profile more similar to experimental results. The difference in the optical absorption between the different geometries and core sizes is also less marked when the clusters are coated. The results suggest that within the 1.4 nm size range, the absorption spectra are dominated by the coating and are not experimentally distinguishable. Binding energies were also calculated for the Au_{55} cluster, showing that the cuboctahedral structure has lower energy although the energy difference was very small. The effect of the coating on the electron density of the gold cluster was also investigated by subtracting the electron densities of the bare clusters from those of the coated clusters (Tsoli *et al.*, 2005; Schmid *et al.*, 1981; Schmid, 1985; Schmid, 2008).

Again, in the nanometre regime, the 55-atom clusters are of particular interest because they correspond to a magic number in the Mackay icosahedron series. However, several theoretical calculations have suggested Au_{55} possessing a disordered amorphous structure as opposed to ordered icosahedrons (Doye & Wales, 1998; Michaelian *et al.*, 1999; Garzón *et al.*, 1998). In 2004, Issendorff and co-workers (Häkkinen *et al.*, 2004) reported systematic high resolution PES spectra of coinage metal clusters Cu_n^- , Ag_n^- and Au_n^- with $n = 53 - 58$. It was observed that while the spectra of Cu_n^- and Ag_n^- were practically identical to each other, Au_n^- clusters displayed completely different spectral patterns. Particularly, the spectra of Cu_{55}^- and Ag_{55}^- were found to be rather simple with several well-separated peaks in the s-band region (corresponding to the delocalized electron shells 1G, 2P and 1F) (Taylor *et al.*, 1992), while that of the Au_{55}^- exhibited one broad (yet congested) band with numerous fine structures. The relatively simple spectral features observed for Cu_{55}^- and Ag_{55}^- are a signature of high-symmetry structures. Comparison of the PES spectra with simulated DOS for a number of candidate structures indeed concluded that Cu_{55}^- and Ag_{55}^- have icosahedral (I_h) ground state structures, whereas the low-lying isomers of Au_{55}^- are all of low symmetries. It was demonstrated that the preference of Au_{55}^- to adopt a low-symmetry structure was due to a relativistic effect, since the reference non-relativistic calculations would give rise to a fictitious (I_h) ground state Au_{55}^- very similar to Cu_{55}^- and Ag_{55}^- .

Huang *et al.* (2008) have carried out a joint PES/DFT investigation of Au_n^- with $n = 55 - 66$, providing a detailed mechanism of how the relativistic effect leads to the low-symmetry structure of Au_{55}^- . Relativistic effects of 5d-6s orbitals of the gold atoms lead to a distortion of the computed geometries of the icosahedral and cubahedral isomers compared to the perfect geometrical shape (Häkkinen *et al.*, 2002; Häkkinen *et al.*, 2004; Häkkinen & Moseler, 2006; Pyykkö, 2004). Because of a better hybridization of the outer shell face center 6s and face edge 6s orbitals, the negatively charged Au_{55}^- cluster has a less distorted geometry than the neutral and positively charged clusters (Periyasamy & Remacle, 2009). Experimentally, the bare Au_{55} clusters are usually stabilized and crystallized in the presence of ligand and solvent layers, which affect their structural and electronic properties. For ligated clusters, the starting geometry of the Au_{55} core was chosen as the stable icosahedral one. This was supported by their previous computations on the $Au_{55}(PH)_{12}Cl_6$ complex where the optimization of cubahedral geometry in the presence of ligands systematically reverts to the distorted icosahedral geometry for all charged states (Periyasamy & Remacle, 2009).

Over all conclusion, Jian *et al.*, (2015) found that the Schmid synthetic route does produce passivated clusters consistent with the formula $Au_{55}(PPh_3)_{12}Cl_6$ clusters as well as clusters containing from about 35 to 60 Au atoms. The fraction of clusters containing 54 ± 1.5 Au atoms, as fractionated by the cluster mass balance (and assuming the standard ligand number), presents atomic structures, measured by aberration corrected STEM which fit best to the hybrid model (42 percent) and amorphous structures (58 percent). They found no evidence of the previously proposed cuboctahedral and icosahedral structures. However the hybrid structure, first proposed for bare Au_{55} , contains both close-packed and icosahedral-type motifs and appears to rationalize the previous contradictory assignments. Looking forward, the combination of size-fractionation by the STEM mass balance method and atomic structure determination in the aberration-correction regime holds promise to reveal the isomeric structures of other nanoparticles (Jian *et al.*, 2015).

3.4. The size effect through the vibrational heat capacity of the cluster Au_{55}

In Figure. 5, we have plotted C_{vib} vs. T at $T = 0.75 - 300K$, in order to prove the size and the temperature influenced effect upon the cluster. Particularly, there is a sudden rise at C_{vib} curve that is due to the starting point of the low frequency of the cluster. Our investigation revealed that the C_{vib} curve is strongly influenced by the temperature, the size, and the structure dependency. Surprisingly, C_{vib} curve is a monotonously increasing function of T (which tends asymptotically). The temperature dependence of the individual modes led to the total vibrational heat capacity for the cluster.

Interestingly, we found that the C_{vib} curve of a neutral gold cluster increases smoothly towards the high temperatures and approaching a constant value, $C_{vib} = 2.80 (2.79586) k_B/atom$ at 300K, and essentially becoming flat. Moreover, the expected absolute value (for size-dependent per atom $-(3N - 6)/N$) should be $C_{vib} = 2.89 k_B/atom$. In our case, the difference is just only $0.09 k_B/atom$ from the absolute value, which is very reasonable within the numerical approach. Nevertheless, at the end, C_{vib} curve almost reached an excellent accurate value, $2.88 (2.88099) k_B/atom$ when

the temperature is high enough, 950 K. With this we can be sure that the structural symmetry can be C_1 for Au_{55} .

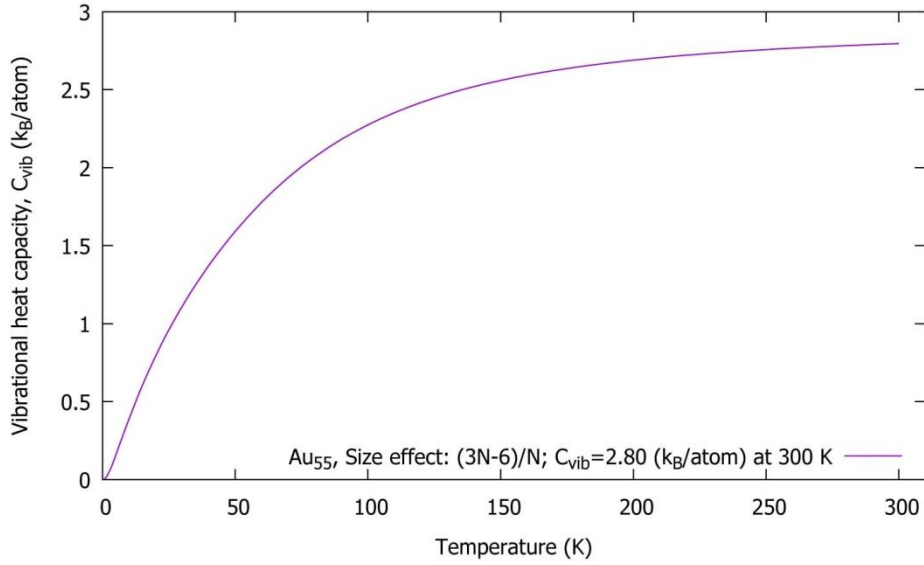


Figure 5. Au_{55} (C_1): The vibrational heat capacity C_{vib} vs. T at 0.75 – 300 K.

3.4.1. The Boson peaks (BP) C_{vib}/T^3 vs. T of the cluster Au_{55}

As shown in Fig. 6, with respect to eqn. (18) and the corresponding Boson peaks C_{vib}/T^2 vs. T and C_{vib}/T^3 vs. T were plotted at the low temperatures $T = 0.75 - 50K$. Some very interesting phenomena being observed, with T^2 at the y -axis the curve reached maximum at the energy values with $0.01 k_B/atom$, at the same time, with T^3 the curve was shrunken and reached the maximum with the lowest energy values in between $0.005 - 0.006 k_B/atom$, but there is no changes occurred on the x -axis, at all. Here, the “hook shape curve” occurrence may be due to the vibrational spectrum starting with consequently double-fold and tripe-fold degeneracy at the beginning of the normal modes of vibrations.

The Boson peak is usually studied in glasses, where enhancement of heat capacity is induced by disorder. The modeling of clusters may be important for understanding the mechanism which leads to this effect. In glasses, there are different local configurations of atoms that may be simulated by isolated clusters. In particular, it was found that the vibrational density of states (VDOS) exhibit an excessively low-frequency contribution. A corresponding low-temperature peak is observed in the temperature dependence of the specific heat if plotted as $C_{vib}(T)/T^3$

Hao Zhang and Jack F. Douglas (Zhang *et al.*, 2010; Zhang & Douglas, 2013) usually studied the Boson peaks from the velocity autocorrelation function, but they are both concerned about an “excess” contribution to the vibrational density of states. This feature has been observed in metal nanoparticles and zeolites (see: Greaves) and attributed to the coordinated harmonic motions of groups of atoms in the boundary region of the particle. There are similarities here to a glass because the surface of a nanoparticle has many features in common with this class of materials. In cases where

the modes have been resolved, the Boson peak has corresponded to a ring of oscillating particles, the relatively low mass being related to the relatively high mass of these modes. Farrusseng & Tuel (2016) also studied the perspectives on zeolite-encapsulated metal nanoparticles and their applications in catalysis.

The increase in C_{vib}/T^3 from $4.62^{-03} k_B/atom$ at $0.75 K$ found for $T \rightarrow 0$ and the maximum deviation at $1.5 K$, finally the Boson curve shows that the exponential decay and reaches towards zero at low temperatures itself, which are due to strong singularities can be found for the TA phonons at the edge atoms on the surface of the clusters. This indicates and confirms a strong disorder nature in the cluster. Moreover, there will be only a minor vibrations at very low temperature, due to the less electrostatic interactions between the nearest neighbouring atoms. Most probably, the acoustic vibrations are more important at low temperatures, because they dominate the heat capacity (Sauceda *et al.*, 2012; Sauceda *et al.*, 2013a; Sauceda *et al.*, 2013b; Sauceda & Garzón, 2015a; Sauceda & Garzón, 2015b; Bravo-Perez *et al.*, 1999a; Bravo-Perez *et al.*, 1999b). Low-frequency modes of harmonic systems can be related to the small amplitude of acoustic waves, which are experimentally observed in all elastic bodies. This implies that, at low temperatures, the specific heat is largely determined by the low frequency part of the vibrational spectrum and it is only at high temperatures that a substantial portion of the spectrum comes into play. However, the acoustic modes will vanish at the longer-wavelength. Therefore, our estimation may be minor longitudinal and transversal sound velocities through the sine-wave anticipated (from eqn. 10-12) by Kieffer (1979a; 1979b), but it will be only possible at the surface of the material.

General view: The bending waves are important due to two reasons. First of all they are mainly responsible for the radiation of sound from vibrating structures since they have a displacement component in the normal direction to the surface of the structure. Secondly, it is the most common wave type when dealing with structure borne sound. At higher frequencies the bending waves change to transversal waves. We assume that the bending waves on atoms, lower frequencies travel slower than the higher frequencies and the form of the signal will therefore be distorted.

To be noticed: Since a very interesting physical phenomena is being observed, let us remember the Figure 5, and the vibrational heat capacity C_{vib} at above $25 K$, raises smoothly (as a linear) and reaches towards $2.80 k_B/atom$ that has showed the size effect values at high temperatures. Similarly, in the Boson peak, C_{vib}/T^3 gets saturated (as a linear) at above $25 K$, but here it towards zero values ($0 k_B/atom$). The lower frequencies certainly make a larger contribution to heat capacity. Nevertheless, the Boson peaks are highly visible, i.e., and the strength of the peaks strongly depends on the atomic coordination number. There are several origins, most of them related to the thermal fluctuations. If the atomic coordination is low, a single negative force constant renders the atomic arrangement much closer to an unstable situation than in the highly coordinated case (Vollath & Luo, 2016; Vollath *et al.*, 2017; Luo *et al.*, 2016).

With the above given detailed information from the many different researchers and their different techniques and our results proven through the size effect, is being an excellent agreements of those conclusion of the non-crystalline, we conclude that $Au_{55}(C_1)$ is definitely of amorphous structure without any doubts.

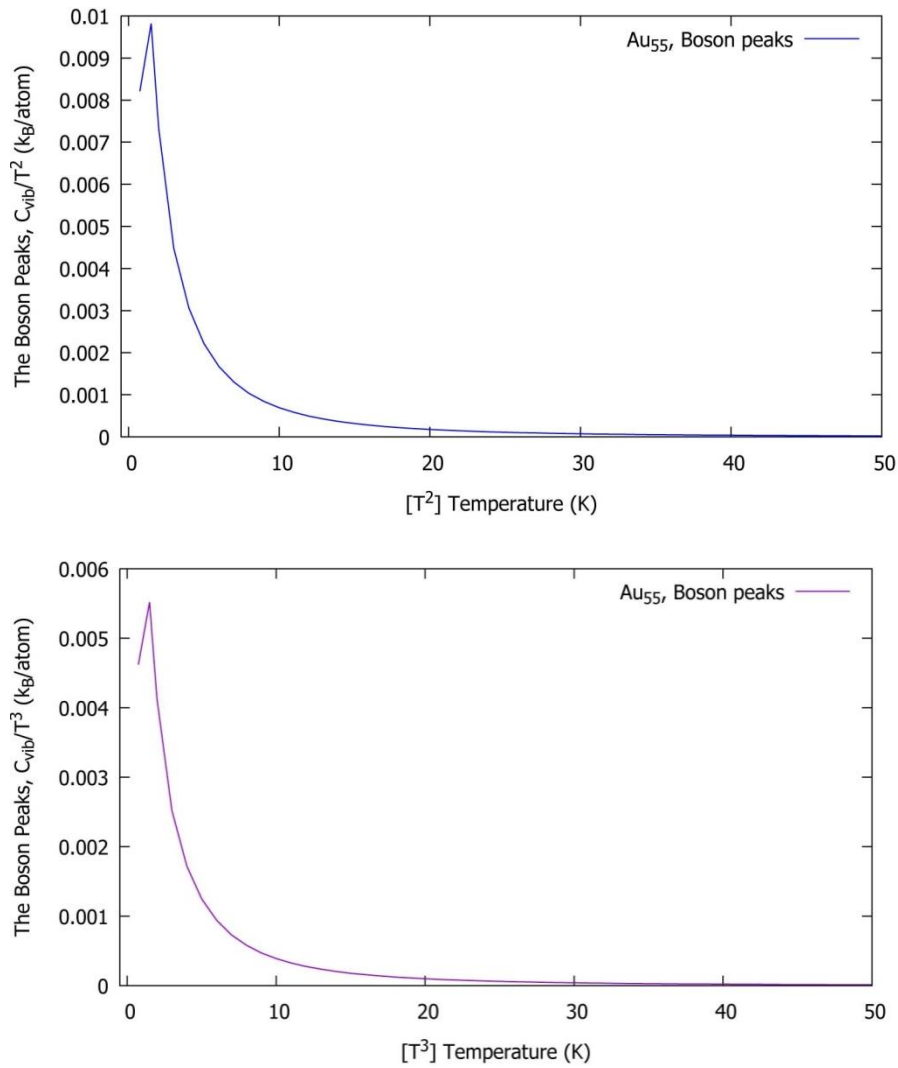


Figure 6. Au_{55} : The Boson peaks C_{vib}/T^2 (top) and C_{vib}/T^3 (bottom) corresponding to the Figure 5

4. Conclusion

We have calculated the vibrational frequency (at $\Delta E = 0$) of a bigger cluster the shell-like structure (they are part of the family of so-called full-shell clusters) and the heat capacity. The ab initio calculations performed within this study confirm the experimental results: The most stable configuration of the Au_{55} cluster is not crystalline but with a high probability this cluster is a shapeless. This cluster was composed of two shells surrounding a central atom. Furthermore, a shell structure should not be considered as a kind of ordering in the context of small nanoparticles. Even the random arrangement of gold atoms, used as starting condition for some of the calculations, shows such a shell structure. In addition to that the structure was confirmed through the size effect, influenced by the heat capacity. We conclude that, the highest probability of the lowest energy structure for Au_{55} can be amorphous (as non-crystalline), which is an excellent agreement with the conclusion of the known results (Doye & Wales 1998;

Huang *et al.*, 2008; Wang L.M. & Wang L.S., 2012; Jian *et al.*, 2015). Moreover, we expect that our amorphous structure will have low toughness, but with high strength at the certain temperatures that was confirmed through the different heat capacity curves (See Fig.5 and Fig. 6).

Last but not least, our present study gives an additional support to the prediction of the existence of shapeless stable structures in metal clusters. The appearance of such structures will always depend on the range of the n-body interaction responsible for the metallic cohesion in these systems. Some similar results to ours have been found in other metal clusters using different semiempirical potentials and ab initio methods. As a consequence, the existence of amorphous clusters does not depend on the use of any specific model potential but on the range and screening of the collective interaction between nuclei and electrons (Garzón & Posada-Amarillas, 1996).

Dedication

Dedicated to Professor David J. Wales ScD, FRSC, FRS, University Chemical Laboratories, Lensfield Road, Cambridge CB2 1EW, United Kingdom, on the occasion of his 55th birthday (as 55 Gold Atomic Clusters), for his extraordinary and distinguished scientific contributions as a young dynamic researcher.

Acknowledgements

Initially, a part of this work was supported by the German Research Council (DFG) through project Sp 439/23-1. We gratefully acknowledge their very generous support.

References

- Alkilany, A.M. & Murphy, C.J. (2010). Toxicity and cellular uptake of gold nanoparticles: what we have learned so far? *Journal of Nanoparticle Research*, 12(7), 2313-2333.
- Baletto, F. & Ferrando, R. (2005). Structural properties of nanoclusters: Energetic, thermodynamic, and kinetic effects. *Reviews of Modern Physics*, 77(1), 371-421 doi:10.1103/RevModPhys.77.371.
- Benfield, R.E., Creighton, J.A., Eadon, D.G. & Schmid, G. (1989). The relationship of $Au_{55}(PPh_3)_{12}Cl_6$ to colloidal gold. *Zeitschrift für Physik D Atoms, Molecules and Clusters*, 12(1-4), 533-536. doi:10.1007/BF01427012
- Bravo-Pérez, G., Garzón, I.L. & Novaro, O. (1999a). Ab initio study of small gold clusters. *Journal of Molecular Structure: THEOCHEM*, 493(1-3), 225-231.
- Bravo-Pérez, G., Garzón, I.L. & Novaro, O. (1999b). Non-additive effects in small gold clusters. *Chemical Physics Letters*, 313(3-4), 655-664.
- Cluskey, P.D., Newport, R.J., Benfield, R.E., Gurman, S.J. & Schmid, G. (1993). An EXAFS study of some gold and palladium cluster compounds. *Zeitschrift für Physik D Atoms, Molecules and Clusters*, 26(1), 8-11. doi:10.1007/BF01425601
- Cox, H., Johnston, R.L. & Murrell, J.N. (1999). Empirical potentials for modeling solids, surfaces, and clusters. *Journal of Solid State Chemistry*, 145(2), 517-540. doi:10.1006/jssc.1999.8200
- D'Agostino, G., Pinto, A. & Mobilio, S. (1993). Simulated gold clusters and relative extended x-ray-absorption fine-structure spectra. *Physical Review B*, 48(19), 14447.

- Darby, S., Mortimer-Jones, T.V., Johnston, R.L. & Roberts, C. (2002). Theoretical study of Cu–Au nanoalloy clusters using a genetic algorithm. *The Journal of Chemical Physics*, 116(4), 1536-1550. doi:10.1063/1.1429658.
- Deaven, D.M. & Ho, K.M. (1995). Molecular geometry optimization with a genetic algorithm. *Physical Review Letters*, 75(2), 288.
- Dong, Y. (2006). Theoretical studies of properties of low-dimensional systems: clusters and conjugated polymers. Ph.D Thesis, Saarland University.
- Dong, Y. & Springborg, M. (2007). Unbiased determination of structural and electronic properties of gold clusters with up to 58 atoms. *The Journal of Physical Chemistry C*, 111(34), 12528-12535.
- Doye, J.P. & Wales, D.J. (1998). Global minima for transition metal clusters described by Sutton–Chen potentials. *New Journal of Chemistry*, 22(7), 733-744.
- Dvornikov, M. (2003). Formulae of numerical differentiation. *arXiv preprint math/0306092*.
- Erkoç, Ş. (2000). Stability of gold clusters: molecular-dynamics simulations. *Physica E: Low-Dimensional Systems and Nanostructures*, 8(3), 210-218. doi:10.1016/S1386-9477(00)00158-2
- Fairbanks, M.C., Benfield, R.E., Newport, R.J. & Schmid, G. (1990). An EXAFS study of the cluster molecule $Au_{55}(PPh_3)_{12}Cl_6$. *Solid State Communications*, 73(6), 431-436. doi:10.1016/0038-1098(90)90045-D
- Farrusseng, D. & Tuel, A. (2016). Perspectives on zeolite-encapsulated metal nanoparticles and their applications in catalysis. *New Journal of Chemistry*, 40(5), 3933-3949.
- Garzon, I.L. & Jellinek, J. (1991). Melting of gold microclusters. *Zeitschrift für Physik D Atoms, Molecules and Clusters*, 20(1), 235-238.
- Garzón, I.L. & Posada-Amarillas, A. (1996). Structural and vibrational analysis of amorphous Au_{55} clusters. *Physical Review B*, 54(16), 11796.
- Garzón, I.L., Michaelian, K., Beltrán, M.R., Posada-Amarillas, A., Ordejón, P., Artacho, E., ... & Soler, J.M. (1998). Lowest energy structures of gold nanoclusters. *Physical Review Letters*, 81(8), 1600-1603.
- Goldberg, D.E. (1989). *Genetic Algorithms in Search, Optimization and Machine Learning*. Addison-Wesley, USA.
- Häkkinen, H., Moseler, M. & Landman, U. (2002). Bonding in Cu, Ag, and Au clusters: relativistic effects, trends, and surprises. *Physical Review Letters*, 89(3), 033401.
- Häkkinen, H., Moseler, M., Kostko, O., Morgner, N., Hoffmann, M.A. & Issendorff, B.V. (2004). Symmetry and electronic structure of noble-metal nanoparticles and the role of relativity. *Physical Review Letters*, 93(9), 093401.
- Häkkinen, H. & Moseler, M. (2006). 55-Atom clusters of silver and gold: Symmetry breaking by relativistic effects. *Computational Materials Science*, 35(3), 332-336.
- Hartke, B. (1995). Global geometry optimization of clusters using a growth strategy optimized by a genetic algorithm. *Chemical Physics Letters*, 240(5-6), 560-565.
- Holland, J.H. (1992). *Adaptation in natural and artificial systems: an introductory analysis with applications to biology, control, and artificial intelligence*. MIT press.
- Hornyak, G.L., Sawitowski, T. & Schmid, G. (1998). TEM, STM and AFM as tools to study clusters and colloids. *Micron*, 29(2-3), 183-190. doi:10.1016/S0968-4328(97)00058-9
- Huang, W., Ji, M., Dong, C.D., Gu, X., Wang, L.M., Gong, X.G. & Wang, L.S. (2008). Relativistic effects and the unique low-symmetry structures of gold nanoclusters. *ACS Nano*, 2(5), 897-904.
- Jellinek, J. & Garzón, I.L. (1991). Structural and dynamical properties of transition metal clusters. *Zeitschrift für Physik D Atoms, Molecules and Clusters*, 20(1), 239-242.

- Jian, N., Stapelfeldt, C., Hu, K.J., Fröba, M., & Palmer, R.E. (2015). Hybrid atomic structure of the Schmid cluster $Au_{55}(PPh_3)_{12}Cl_6$ resolved by aberration-corrected STEM. *Nanoscale*, 7(3), 885-888.
- Jin, R. (2010). Quantum sized, thiolate-protected gold nanoclusters. *Nanoscale*, 2, 343-362 DOI: 10.1039/b9nr00160c.
- Joswig, J.-O. (2003). Theoretical Studies of Properties of Clusters, PhD Thesis, Saarland University.
- Jun, Y., Zhen-An, T., Feng-Tian, Z., Guang-Fen, W. & Li-Ding, W. (2005). Investigation of a microcalorimeter for thin-film heat capacity measurement. *Chinese Physics Letters*, 22(9), 2429.
- Kieffer, S.W. (1979a). Thermodynamics and lattice vibrations of minerals: 1. Mineral heat capacities and their relationships to simple lattice vibrational models. *Reviews of Geophysics*, 17(1), 1-19.
- Kieffer, S.W. (1979b). Thermodynamics and lattice vibrations of minerals: 2. Vibrational characteristics of silicates. *Reviews of Geophysics*, 17(1), 20-34.
- Krakow, W., José-Yacamán, M., & Aragón, J. L. (1994). Observation of quasimelting at the atomic level in *Au* nanoclusters. *Physical review B*, 49(15), 10591.
- Li, T.X., Ji, Y.L., Yu, S.W. & Wang, G.H. (2000). Melting properties of noble metal clusters. *Solid State Communications*, 116(10), 547-550. doi:10.1016/S0038-1098(00)00373-2.
- Luo, P., Li, Y.Z., Bai, H.Y., Wen, P., & Wang, W.H. (2016). Memory effect manifested by a boson peak in metallic glass. *Physical Review Letters*, 116(17), 175901.
- Marcus, M.A., Andrews, M.P., Zegenhagen, J., Bommannavar, A.S. & Montano, P. (1990). Structure and vibrations of chemically produced Au_{55} clusters. *Physical Review B*, 42(6), 3312.
- Michaelian, K., Rendón, N. & Garzón, I.L. (1999). Structure and energetics of *Ni*, *Ag*, and *Au* nanoclusters. *Physical Review B*, 60(3), 2000.
- Morris, J.R., Deaven, D.M. & Ho, K.M. (1996). Genetic-algorithm energy minimization for point charges on a sphere. *Physical Review B*, 53(4), R1740.
- Murray, R.W. (2008). Nanoelectrochemistry: Metal nanoparticles, nanoelectrodes and nanopores. *Chem. Rev.*, 108(7), 2688-2720.
- Novotny, V., Meincke, P.P.M. & Watson, J.H.P. (1972). Effect of size and surface on the specific heat of small lead particles. *Physical Review Letters*, 28(14), 901.
- Periyasamy, G. & Remacle, F. (2009). Ligand and solvation effects on the electronic properties of Au_{55} clusters: A density functional theory study. *Nano Lett.*, 9(8), 3007-3011.
- Pinto, A., Pennisi, A.R., Faraci, G., D'agostino, G., Mobilio, S. & Boscherini, F. (1995). Evidence for truncated octahedral structures in supported gold clusters. *Physical Review B*, 51(8), 5315.
- Porezag, D., Frauenheim, T., Köhler, T., Seifert, G., & Kaschner, R. (1995). Construction of tight-binding-like potentials on the basis of density-functional theory: Application to carbon. *Physical Review B*, 51(19), 12947.
- Pyykkö, P. (2004). Theoretical chemistry of gold. *Angewandte Chemie International Edition*, 43(34), 4412-4456.
- Roberts, C., Johnston, R.L. & Wilson, N.T. (2000). A genetic algorithm for the structural optimization of Morse clusters. *Theoretical Chemistry Accounts*, 104(2), 123-130.
- Rose, J.P. & Berry, R.S. (1993). $(KCl)_{32}$ and the possibilities for glassy clusters. *The Journal of Chemical Physics*, 98(4), 3262-3274.

- Sachdev, A., Masel, R.I. & Adams, J.B. (1993). An embedded atom method study of the equilibrium shapes of small platinum and palladium clusters. *Zeitschrift für Physik D Atoms, Molecules and Clusters*, 26(1), 310-312.
- Sauceda, H.E., Mongin, D., Maioli, P., Crut, A., Pellarin, M., Del Fatti, N., ... & Garzón, I.L. (2012). Vibrational properties of metal nanoparticles: Atomistic simulation and comparison with time-resolved investigation. *The Journal of Physical Chemistry C*, 116(47), 25147-25156.
- Sauceda, H.E., Pelayo, J.J., Salazar, F., Pérez, L.A. & Garzón, I.L. (2013a). Vibrational spectrum, caloric curve, low-temperature heat capacity, and debye temperature of sodium clusters: The Na_{139}^+ case. *The Journal of Physical Chemistry C*, 117(21), 11393-11398.
- Sauceda, H.E., Salazar, F., Pérez, L.A. & Garzón, I. L. (2013b). Size and shape dependence of the vibrational spectrum and low-temperature specific heat of Au nanoparticles. *The Journal of Physical Chemistry C*, 117(47), 25160-25168.
- Sauceda, H.E. & Garzón I.L., (2015a). Structural determination of metal nanoparticles from their vibrational (Phonon) density of states. *J. Phys. Chem. C.*, 119, 10876.
- Sauceda, H.E. & Garzón, I.L. (2015b). Vibrational properties and specific heat of core-shell Ag-Au icosahedral nanoparticles. *Physical Chemistry, Chemical Physics*, 17(42), 28054-28059.
- Sawada, S. & Sugano, S. (1991). Theory of the structural fluctuation of Au_{55} clusters. *Zeitschrift für Physik D Atoms, Molecules and Clusters*, 20(1), 259-261. doi:10.1007/BF01543987.
- Sawada, S. & Sugano, S. (1992). Structural fluctuation of Au_{55} and Au_{147} clusters: Substrate effect. *Zeitschrift für Physik D Atoms, Molecules and Clusters*, 24(4), 377-384.
- Schmid, G., Pfeil, R., Boese, R., Bandermann, F., Meyer, S., Calis, G.H. & van der Velden, J. W. (1981). $Au_{55}[P(C_6H_5)_3]_{12}Cl_6$ -ein Goldcluster ungewöhnlicher Größe. *Chemische Berichte*, 114(11), 3634-3642.
- Schmid, G. (1985). Developments in transition metal cluster chemistry - the way to large clusters. In *Clusters* (pp. 51-85). Springer, Berlin, Heidelberg. doi:10.1007/BFb0009185.
- Schmid, G. (2008). The relevance of shape and size of Au_{55} clusters. *Chemical Society Reviews*, 37(9), 1909-1930. doi:10.1039/b713631p.
- Seifert, G. & Schmidt, R. (1992). Molecular dynamics and trajectory calculations: the application of an LCAO-LDA scheme for simulations of cluster-cluster collisions. *New Journal of Chemistry*, 16(12), 1145-1147.
- Seifert, G., Porezag, D. & Frauenheim, T. (1996). Calculations of molecules, clusters, and solids with a simplified LCAO-DFT-LDA scheme. *International Journal of Quantum Chemistry*, 58(2), 185-192.
- Seifert, G. (2007). Tight-binding density functional theory: an approximate Kohn-Sham DFT scheme. *The Journal of Physical Chemistry A*, 111(26), 5609-5613.
- Simon, U., Schon, G. & Schmid, G. (1993). The Application of Au_{55} clusters as quantum dots. *Angew. Chem., Int. Ed.*, 32(2), 250-254.
- Song, Q., Cui, Z., Xia, S. & Chen, S. (2004). An AC microcalorimeter for measuring specific heat of thin films. *Microelectronics Journal*, 35(10), 817-821.
- Taylor, K.J., Pettiette-Hall, C.L., Cheshnovsky, O. & Smalley, R.E. (1992). Ultraviolet photoelectron spectra of coinage metal clusters. *The Journal of Chemical Physics*, 96(4), 3319-3329.
- Tsoli, M., Kuhn, H., Brandau, W., Esche, H. & Schmid, G. (2005). Cellular uptake and toxicity of Au_{55} clusters. *Small*, 1(8-9), 841-844.
- Vishwanathan, K. (2016). Vibrational heat capacity of gold cluster $Au_N = 14$ at low temperatures. *J. Phys. Chem. Biophys*, 6, 1-5.

- Vishwanathan, K. (2017a). Effect of size, temperature, and structure on the vibrational heat capacity of small neutral gold clusters. *J. Mater. Sci. Eng*, 6, 325.
- Vishwanathan, K. (2017b). Does the Boson peaks exist in small neutral gold clusters? *J. Develop. Drugs.*, 6, 178. doi:10.4172/2329-6631.1000178.
- Vishwanathan, K. (2017c). Symmetry of gold neutral clusters Au_{3-20} and normal modes of vibrations by using the numerical finite difference method with density-functional tight-binding (DFTB) approach. *Arch. Chem. Res.*, 1(3), 17. doi: 10.21767/2572-4657.100017.
- Vishwanathan, K. (2018). Bonding forces and energies on the Potential Energy Surface (PES) of the optimized gold atomic clusters by a differentiation step-size ($ds = \pm 0.01$ a.u.) via DFTB Method. *Nanoscience & Technology Open Access*, 5(2), 1-4. doi: 10.15226/2374-8141/5/2/00159.
- Vogel, W., Rosner, B. & Tesche, B. (1993). Structural investigations of gold (Au_{55}) organometallic complexes by x-ray powder diffraction and transmission electron microscopy. *The Journal of Physical Chemistry*, 97(45), 11611-11616.
- Vollath, D. & Fischer, F.D. (2014). Estimation of Thermodynamic Data of Metallic Nanoparticles Based on Bulk Values. *Metal Nanopowders: Production, Characterization, and Energetic Applications*, 1-24. doi:10.1002/9783527680696.ch1
- Vollath, D., Holec, D. & Fischer, F.D. (2017). Au_{55} , a stable glassy cluster: results of ab initio calculations. *Beilstein Journal of Nanotechnology*, 8(1), 2221-2229.
- Wallenberg, L.R., Bovin, J.O. & Schmid, G. (1985). On the crystal structure of small gold crystals and large gold clusters. *Surface Science*, 156, 256-264.
- Wang, L.M. & Wang, L.S. (2012). Probing the electronic properties and structural evolution of anionic gold clusters in the gas phase. *Nanoscale*, 4(14), 4038-4053.
- Wang, Z.W. & Palmer, R.E. (2012). Experimental evidence for fluctuating, chiral-type Au_{55} clusters by direct atomic imaging. *Nano letters*, 12(11), 5510-5514. doi: 10.1021/nl303429z.
- Warnke, I. (2007). Heat Capacities of Metal Clusters, Diploma Thesis (Research Assistant and Diploma Research), Saarland University.
- Yam, V.W.W. & Cheng, E.C.C. (2008). Highlights on the recent advances in gold chemistry a photophysical perspective. *Chem. Soc. Rev.*, 37(9), 1806-1813.
- Yao, L., Qing-Lin, S. & Shan-Hong, X. (2005). Calculation of specific heat for aluminium thin films. *Chinese Physics Letters*, 22(9), 2346.
- Yi, J.Y., Oh D.J. & Bernholc J., (1991). Structural distortions in metal clusters. *Physical Review Letters*, 67, 1594-1597.
- Yildirim, E.K. & Guvenç, Z.B. (2006). Differences in melting behaviours of disordered and symmetric clusters: Au_N ($N = 54-56$). *Modelling and Simulation in Materials Science and Engineering*, 14(6), 947-961. doi:10.1088/0965-0393/14/6/005
- Yu, X. & Duxbury, P.M. (1995). Kinetics of nonequilibrium shape change in gold clusters. *Physical Review B*, 52(3), 2102.
- Zhang, H., Kalvapalle, P. & Douglas, J.F. (2010). String-like collective atomic motion in the interfacial dynamics of nanoparticles. *Soft Matter*, 6(23), 5944-5955.
- Zhang, H. & Douglas, J.F. (2013). Glassy interfacial dynamics of Ni nanoparticles: Part II discrete breathers as an explanation of two-level energy fluctuations. *Soft Matter*, 9(4), 1266-1280.